Is the Electrostatic Blob Model Relevant to Dilute Polyelectrolyte Solutions Undergoing Shear Flow?

S. K. Pattanayek[†] and J. Ravi Prakash*

Department of Chemical Engineering, Monash University, Melbourne VIC 3800 Australia

Received September 20, 2007; Revised Manuscript Received December 31, 2007

ABSTRACT: The equilibrium behavior of dilute polyelectrolyte solutions has previously been successfully described by scaling theories based on the electrostatic blob model of de Gennes et al. in terms of just two scaling variables: the number of blobs *X*, and the Debye screening length relative to the size of the blob *Y*, where both *X* and *Y* are determined from the properties of the polyelectrolyte, and the solvent. We show, in the context of Brownian dynamics simulations, that (i) the scaling picture at equilibrium can be accurately reproduced by a bead−spring chain model and that, (ii) with the inclusion of the characteristic shear rate β as the additional scaling variable in shear flow, the equilibrium blob model provides a framework to obtain parameter free data collapse, even for rheological properties. As a result, regardless of the degree of coarse-graining, i.e., the number of beads *N* in the bead spring chain model (provided $N \geq X$), identical results for the shear rate dependence of viscosity are obtained, so long as *X*, *Y*, and β are the same.

1. Introduction

Polyelectrolyte solutions exhibit a significantly more varied and complex behavior than solutions of uncharged polymers because their properties depend on a number of additional parameters. For instance, apart from the number of monomers in a chain, the persistence length, and the solvent quality for the polymer backbone, which are the parameters that determine the static behavior of linear homopolymers, extra factors such as the fraction of disassociated ionic groups, the charge valency of these groups, the dielectric constant of the solution, and the concentration of counterions and salt ions in the solution, play an important role in governing the rich behavior observed in polyelectrolyte solutions.[1,2] Consequently, the success of scaling theories built on the electrostatic blob model of de Gennes et al.[3] in achieving a coherent representation of experimental and simulation data of dilute polyelectrolyte solutions at equilibrium, in terms of a vastly reduced number of scaling variables, is remarkable.[4,5] The aim of the present paper is to examine whether the equilibrium blob model of de Gennes et al. is useful as a framework to obtain a parameter free representation of Brownian dynamics simulation data for the properties of dilute polyelectrolyte solutions, in a far from equilibrium situation such as shear flow.

In most scaling theories, polyelectrolyte molecules are represented by polymer chains with N_k monomers, each with length b_k, and the extent of ionic group disassociation is taken into account by assuming that only some monomers, separated by *s* monomer units along the length of the chain, are charged. The solvent molecules are replaced by a continuum, characterized by a Bjerrum length l_B (which is the distance at which the Coulomb energy between two unit charges in the solvent is equal to the thermal energy k_BT). The counterions and salt ions are typically not considered explicitly, but instead, are treated as an effective background leading to screened electrostatic interactions between charges on the chain, with a Debye screening length l_D that depends on the concentration of small ions. The basic assumption of the blob model is that the conformation of a polyeleetrolyte chain is unaffected by electrostatic interactions on short length scales, since the total interaction in a short chain segment is small. The scale at which electrostatic interactions become important is represented by the size of the blob, with the conformation of the chain pictured as a chain of blobs, as displayed in the upper half of Figure 1. Indeed, both the size of the blob ξ and the number of blobs *X* in the chain are estimated by evaluating the conditions under which two neighboring blobs have an electrostatic repulsion of order k_BT.[4−6] In the blob model, the entire set of "bare" model parameters $\{N_k, b_k, s, l_B, l_D\}$ is replaced by just two scaling variables,[4] the number of blobs

$$X = \frac{N_k}{(\xi/b_k)^2} \tag{1}$$

and the reduced screening length

$$Y = \frac{l_D}{\xi} \tag{2}$$

where

$$\frac{\xi}{b_k} = \frac{s^{2/3}}{(l_B/b_k)^{1/3}} \tag{3}$$

Within this framework, static properties are completely determined by a specification of *X* and *Y*. For instance, the scaling behavior of the nondimensional end-to-end vector $\langle r^2\rangle/\xi^2$, in the *X* and *Y* parameter space, can be represented in terms of a phase-diagram, as displayed in Figure 2. Figure 2, which has been composed based on a similar figure in ref 4, will be discussed in greater detail in section 3. The point to be noted here is that, over the years, several simulation studies have clearly demonstrated the validity of the blob model and the resultant scaling picture (see refs 4,5 and references therein).

The focus of the present paper is on simulating the rheological behavior of dilute polyelectrolyte solutions. In the case of dilute solutions of *uncharged* linear homopolymers, the past decade

* Corresponding author. E-mail: Ravi.Jagadeeshan@eng.monash.edu.au.
[†] Presently at Department of Chemical Engineering, Indian Institute of Technology, Delhi, India. E-mail: sudip@chemical.iitd.ac.in.

10.1021/ma702114u CCC: $40.75
Published on Web 02/19/2008

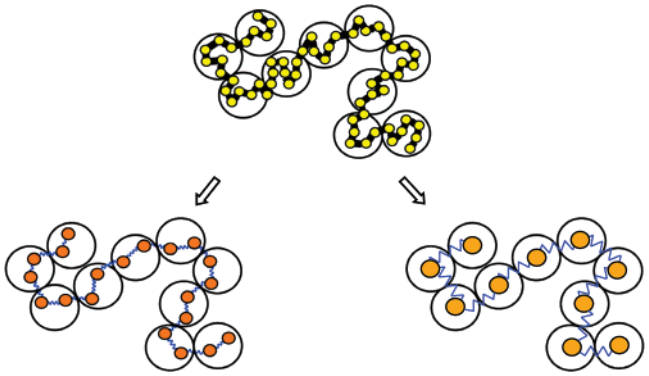

Figure 1. Representation of a polyelectrolyte by a chain of electrostatic blobs, and two coarse-grained bead−spring chain representations that preserve the conformation of the blob chain.

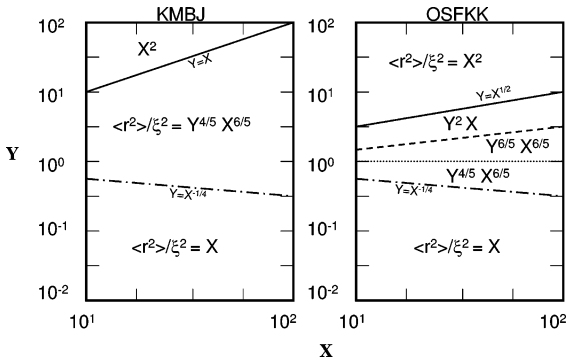

Figure 2. Phase-diagram of the various conformational states of a polyelectrolyte chain represented in terms of the scaling behavior of the nondimensional end-to-end vector $\langle r^2\rangle/\xi^2$, as a function of the number of blobs X and the reduced screening length Y. The two distinct scaling theory predictions have been denoted by the initials of the main authors of these theories, following Everaers et al.,[4] as KMBJ[7−10] and OSFKK.[11−13]

has seen significant advances in our capacity to understand and predict their rheological behavior.[14,15] Basically, a polymer chain with N_k Kuhn steps, each of length b_k, is represented by a coarse-grained model, typically a bead−spring chain consisting of N beads, connected to each other by linear Hookean or nonlinear finitely extensible springs. Closure approximations[16−18] and Brownian dynamics simulations (BDS)[19−26] based on molecular theories developed with polymer kinetic theory[27] have proven to be invaluable in obtaining nearly quantitative predictions of material properties in shear and extensional flows. Though an attempt to use a similar approach to describe the rheology of dilute polyelectrolyte solutions was made several years ago in the seminal paper by Dunlap and Leal,[28] subsequent rheological investigations have been sporadic and far apart, and only recently have more studies exploiting the power of BDS begun to appear in the literature.[29−31] In an alternative approach, using a scaling theory based on the electrostatic blob model, Borisov et al.[32] have predicted the behavior of dilute polyelectrolyte solutions in elongational flows. More recently, Colby et al.[33] have used the notion of a deformed Pincus blob[34,35] in order to modify Rouse theory, and as a result, obtain a prediction for the shear rate dependence of the viscosity of semidilute unentangled polyelectrolyte solutions. However, in contrast to the situation for equilibrium properties, there has been no attempt so far, to our knowledge, to examine with the help of rigorous simulations, whether the electrostatic blob model continues to be a useful framework in far from equilibrium situations. The question that lies at the heart of the present work can be posed in terms of the cartoon represented in Figure 1. If varied levels of coarse-graining of the bead−spring chain model are used, provided the basic blob conformation at equilibrium is maintained, will the behavior observed in shear flow be identical? Of course, it can be anticipated that a scaling variable in addition to X and Y will be necessary to characterize the flow. A commonly used scaling variable to collapse data for polymers of different molecular weights in shear flows is the characteristic shear rate β, defined as $\beta = \lambda_p\dot{\gamma}$, where $\dot{\gamma}$ is the shear rate and λ_p is a characteristic relaxation time defined by[27]

$$\lambda_p = \frac{[\eta]_0 M \eta_s}{N_A k_B T} \tag{4}$$

Here, $[\eta]_0$ is the zero shear rate intrinsic viscosity, M is the molecular weight, η_s is the solvent viscosity, and N_A is Avogadro's number.

The existence of a description independent of the level of coarse-graining has significant implications for the comparison of simulation results with experiments. One of the vexatious issues in the use of BDS to describe polymer solution rheology is the rational choice of the various parameters that appear in the bead−spring chain model. For dilute polyelectrolyte solutions, Pamies et al.[30] in their recent paper have suggested a method for calculating the parameters in the Debye−Hückel interaction potential from experimental data. However, their choice of the number of beads in the bead−spring chain N remains arbitrary. For uncharged polymers under free-draining conditions in a Θ-solvent, Underhill and Doyle[36] have developed an approach to coarse-graining where the accuracy of the bead−spring chain model can be made independent of the choice of N. Under more general conditions, where hydrodynamic interactions and excluded volume effects are taken into account, Prakash and co-workers have developed the successive fine-graining procedure, which has been shown to lead to parameter free predictions.[23,24,37,38] The success of this approach is based on exploiting the two-parameter theory for dilute polymer solutions,[39] and would consequently need modification to account for the additional physics in dilute polyelectrolyte solutions. The electrostatic blob model provides an appealing alternative approach to parameter free predictions. Clearly, the values of the scaling variables X, Y, and β can be relatively easily determined from experimental data characterizing the polyelectrolyte chain, the solvent, and the flow. If BDS data can be represented in terms of these scaling variables, then predictions independent of the choice of parameters in the bead−spring chain model can be obtained. The aim of this paper is to systematically investigate whether such an approach is successful.

The structure of the paper is as follows. In section 2, we describe the model for polyelectrolyte solutions used here, and discuss the scheme for mapping bead−spring chain model parameters onto the relevant scaling variables. In section 3, we show how the electrostatic blob model can be used to represent BDS data for the equilibrium end-to-end vector in terms of only the scaling variables X and Y. We also compare our results with earlier work on equilibrium properties. In section 4, we establish the usefulness of the blob model in collapsing data for the viscosity of dilute polyelectrolyte solutions obtained from BDS. We examine both the free-draining situation and the case where hydrodynamic interactions are included. Finally, we summarize our conclusions in section 5.

2. Mapping the Bead−Spring Chain onto the Blob Model

A dilute polyelectrolyte solution is modeled here as an ensemble of noninteracting bead−spring chains, each with N

beads connected by FENE springs, dissolved in a solvent, with the solvent molecules replaced by a continuum. It is assumed that each charged monomer on the polyelectrolyte chain carries unit charge. This implies that for any choice of N, the charge on each bead is given by

$$q = \frac{N_k}{sN} \tag{5}$$

The time evolution of the configurational distribution function $\psi(\mathbf{r}_1, ..., \mathbf{r}_N, t)$ of the bead positions $\mathbf{r}_\mu$, is governed by the Fokker−Planck equation:[19,27,40]

$$\frac{\partial \psi}{\partial t} = -\sum_{\mu=1}^{N} \frac{\partial}{\partial \mathbf{r}_\mu}\left[\boldsymbol{\kappa}\cdot\mathbf{r}_\mu + \frac{1}{\zeta}\sum_{\nu=1}^{N} \boldsymbol{\Gamma}_{\mu\nu}\cdot(\boldsymbol{F}_\nu^s + \boldsymbol{F}_\nu^{int})\right]\psi + \frac{k_B T}{\zeta}\sum_{\mu,\nu=1}^{N} \frac{\partial}{\partial \mathbf{r}_\mu}\cdot\boldsymbol{\Gamma}_{\mu\nu}\cdot\frac{\partial \psi}{\partial \mathbf{r}_\nu} \tag{6}$$

Here, $\boldsymbol{\kappa}$ is the time-dependent, homogeneous, velocity gradient tensor, ζ is the hydrodynamic friction coefficient associated with a bead, and $\boldsymbol{\Gamma}_{\nu\mu}$ is the dimensionless diffusion tensor that is related to the hydrodynamic interaction (HI) tensor $\boldsymbol{\Omega}_{\nu\mu}$ through $\boldsymbol{\Gamma}_{\nu\mu} = \delta_{\nu\mu}\delta + \zeta\boldsymbol{\Omega}_{\nu\mu}$. $\boldsymbol{\delta}$ and $\boldsymbol{\delta}_{\mu\nu}$ represent a unit tensor and a the Kronecker delta, respectively, and the hydrodynamic interaction tensor $\boldsymbol{\Omega}_{\nu\mu}$ represents the effect of the motion of a bead μ on another bead ν through the disturbances carried by the surrounding fluid. Several recent investigations have established that it is crucial to include HI effects in order to predict dynamic and rheological properties of polymer solutions accurately.[20−26,37] The specific form used here is discussed shortly below. $\boldsymbol{F}_\nu^s$ is the spring force on bead ν due to adjacent beads, $\boldsymbol{F}_\nu^s = \boldsymbol{F}^c(\mathbf{Q}_\nu) - \boldsymbol{F}^c(\mathbf{Q}_{\nu-1})$, where $\boldsymbol{F}^c(\mathbf{Q}_{\nu-1})$ is the force between the beads $\nu - 1$ and ν, acting in the direction of the connector vector between the two beads $\mathbf{Q}_{\nu-1} = \mathbf{r}_\nu - \mathbf{r}_{\nu-1}$. The quantity $\boldsymbol{F}_\mu^{int}$ is the total electrostatic interaction force on bead μ due to all the other beads, $\boldsymbol{F}_\mu^{int} = \sum_{\nu=1}^{N} \boldsymbol{F}^{el}(\mathbf{r}_{\mu\nu})$, where $\boldsymbol{F}^{el}$ is the electrostatic interaction force acting along the vector $\mathbf{r}_{\mu\nu} = \mathbf{r}_\nu - \mathbf{r}_\mu$ connecting beads μ and ν. $\boldsymbol{F}^{el}$ can be derived from the electrostatic interaction potential ϕ^{el}

$$\boldsymbol{F}^{el}(\mathbf{r}_{\mu\nu}) = -\frac{\partial \phi^{el}(r_{\mu\nu})}{\partial \mathbf{r}_{\mu\nu}} \tag{7}$$

where $r_{\mu\nu} = |\mathbf{r}_{\mu\nu}|$. Note that, within this basic structure, it is straightforward to account for the influence of solvent quality effects through the use of a pairwise excluded volume force between the beads.[24,37] However, as pointed out by Everaers et al.,[4] since some of the controversy surrounding the predictions of equilibrium theories might be related to the difficulty in separating out the influence of electrostatic and excluded volume (EV) effects in polyelectrolyte solutions, we have not included EV here, and focus our attention instead on studying the role of electrostatic interactions alone, in a solution which is under Θ conditions for the uncharged polymer. In molecular simulations of dilute solutions, a representation of the Θ state (where the two and three-body intramolecular interactions compensate each other, and the chain behaves ideally), is typically captured in two distinct ways. The first approach, consists of carefully selecting parameter values in the *pairwise* excluded volume interaction potential such that attractive forces exactly balance repulsive interactions. This method is often implemented in molecular dynamics simulations in which the solvent is modeled explicitly, and requires significant effort in determining the correct parameters−particularly in the simulation of new systems. In the second method, often used in Brownian dynamics simulations, the Θ state is achieved simply by not including excluded volume effects at all in the model. This method has been previously successfully applied to study linear polymers and has been shown to lead to the correct prediction of scaling laws in the Θ state, and to agreements with the predictions of the Rouse and Zimm theories. We assume in our work that Θ conditions imply that all segments of the polymer behave ideally, and following previous Brownian dynamics simulations, we set the excluded volume interactions to be zero.

The mean-square end-to-end vector $\langle r^2 \rangle$ of a polyelectrolyte chain is the only static property examined in this work. It is defined by $\langle r^2 \rangle = \langle \mathbf{r}_{1,N}{}^2 \rangle$, and is related to the second moments of the spring connector vectors through

$$\langle r^2 \rangle = \sum_{i,j=1}^{N} \mathrm{tr}\langle \mathbf{Q}_i \mathbf{Q}_j \rangle \tag{8}$$

where the angular brackets indicate averages over the distribution functionm ψ.

The only far from equilibrium situation considered here is steady simple shear flow, which is specified by the following matrix representation for the tensor $\boldsymbol{\kappa}$ in a laboratory-fixed coordinate system

$$\boldsymbol{\kappa} = \dot{\gamma}\begin{pmatrix} 0 & 1 & 0 \\ 0 & 0 & 0 \\ 0 & 0 & 0 \end{pmatrix} \tag{9}$$

where as mentioned earlier, $\dot{\gamma}$ is the constant shear rate.

Once the components of the stress tensor, τ_{xy}^p, τ_{xx}^p, etc., are known, the viscosity η_p, and the first normal stress difference coefficient Ψ_1, can be obtained from the following relations:[41]

$$\tau_{xy}^p = -\dot{\gamma}\eta_p;\ \tau_{xx}^p - \tau_{yy}^p = -\dot{\gamma}^2\Psi_1 \tag{10}$$

For constraint-free models with arbitrary intramolecular forces, $\boldsymbol{\tau}^p$ is given by the *Kramers* expression[27]

$$\boldsymbol{\tau}^p = (N-1)n_p k_B T\,\delta + n_p \sum_{\nu=1}^{N} \langle \boldsymbol{R}_\nu (\boldsymbol{F}_\nu^s + \boldsymbol{F}_\nu^{int})\rangle \tag{11}$$

where n_p is the number density of the polymer solution, and $\boldsymbol{R}_\nu = \mathbf{r}_\nu - \mathbf{r}_c$ is the position vector of the νth bead relative to the position of the center of mass of the chain, $\mathbf{r}_c = (1/N)\sum_{\mu=1}^{N} \mathbf{r}_\mu$.

The following nondimensionalization scheme is adopted here: all lengths are nondimensionalized with respect to the length scale l_H, defined as $l_H = \sqrt{k_B T/H}$, time is nondimensionalized with respect to relaxation time λ_H, defined as $\lambda_H = \zeta/4H$, energy by $k_B T$, and force by $\sqrt{H k_B T}$, where H is the spring constant. Dimensionless quantities are denoted with an asterisk as superfix; for instance, $\mathbf{r}_{\mu\nu}^* = \mathbf{r}_{\mu\nu}/l_H$.

Within this framework, the nondimensional connector force for a FENE spring is given by

$$\boldsymbol{F}^{c*}(\mathbf{Q}^*) = \left(\frac{1}{1 - \mathbf{Q}^{*2}/b}\right)\mathbf{Q}^* \tag{12}$$

where $b = Q_0{}^2/l_H{}^2$, is the FENE parameter, with Q_0 representing the fully stretched length of a spring. For a given choice of N, a comparison of both the equilibrium end-to-end vector and the fully stretched length of the bead−spring chain, with identical properties for the underlying polymer chain (with N_k Kuhn steps of length b_k), leads to[24]

$$b = 3\frac{N_k}{N-1} - 5 \tag{13}$$

The hydrodynamic interaction tensor used here is the Rotne−Prager−Yamakawa (RPY) interaction tensor,[42] which is given in a nondimensional form by

$$\Omega(\mathbf{r}^*) = \left[\Omega_1 \boldsymbol{\delta} + \Omega_2 \frac{\mathbf{r}^*\mathbf{r}^*}{r^{*2}}\right] \tag{14}$$

where for $r^* \geq 2\sqrt{\pi}h^*$

$$\Omega_1 = \frac{3\sqrt{\pi}}{4}\frac{h^*}{r^*}\left(1 + \frac{2\pi}{3}\frac{h^{*2}}{r^{*2}}\right); \quad \Omega_2 = \frac{3\sqrt{\pi}}{4}\frac{h^*}{r^*}\left(1 - 2\pi\frac{h^{*2}}{r^{*2}}\right)$$

and for $0 < r^* \leq 2\sqrt{\pi}h^*$

$$\Omega_1 = 1 - \frac{9}{32}\frac{r^*}{h^*\sqrt{\pi}}; \quad \Omega_2 = \frac{3}{32}\frac{r^*}{h^*\sqrt{\pi}}$$

In deriving the above expressions, the Stokes drag formula $\zeta = 6\pi\eta_s a$, for a spherical bead of radius a, has been used. The quantity h^*, known as the hydrodynamic interaction parameter, is the nondimensional radius of the bead defined by

$$h^* \equiv \frac{a}{\sqrt{\pi}l_H} \tag{15}$$

As in earlier scaling theories, we assume that the electrostatic interaction force is derived from a Debye−Hückel screened electrostatic interaction potential

$$\phi^{el^*}(r^*_{\mu\nu}) = \frac{q^2 l^*_B}{r^*_{\mu\nu}}\exp(-r^*_{\mu\nu}/l^*_D) \tag{16}$$

With these redefined expressions, the nondimensional diffusion equation can be written as

$$\frac{\partial\psi}{\partial t^*} = \sum_{\mu,\nu=1}^{N}\frac{\partial}{\partial\mathbf{r}^*_\mu}\cdot\boldsymbol{\Gamma}_{\mu\nu}(h^*)\cdot\frac{\partial\psi}{\partial\mathbf{r}^*_\nu} - \sum_{\mu=1}^{N}\frac{\partial}{\partial\mathbf{r}^*_\mu}\Bigg[\kappa^*(\dot{\gamma}^*)\cdot\mathbf{r}^*_\mu + \sum_{\nu=1}^{N}\boldsymbol{\Gamma}_{\mu\nu}(h^*)\cdot(\boldsymbol{F}^{s^*}_\nu(b) + \boldsymbol{F}^{int^*}_\nu(q, l^*_B, l^*_D))\Bigg]\psi \tag{17}$$

where the dependence of the functions on the various parameters has been displayed explicitly for future reference.

The exact solution of the time evolution of various averages carried out with the distribution function ψ, without any further approximations, can be obtained by writing a stochastic differential equation (SDE) equivalent to eq 17 and solving it with the help of a Brownian dynamics algorithm.[19] In the presence of fluctuating HI, the problem of the computational intensity of calculating the Brownian term has been attenuated significantly recently[43] by the use of a Chebyshev polynomial representation[44] for the Brownian term. We have adopted this strategy, and the details of the exact algorithm followed here are given in ref 22. The problem of the large error in BD simulations at low shear rates has been overcome by adopting a variance reduction procedure.[45,46]

As mentioned earlier, the scaling variables X and Y can be determined from the values of the bare parameters. Indeed it suffices to know values of the set of variables $\{N_k, s, l_B/b_k, l_D/b_k\}$, without an explicit knowledge of b_k. Equilibrium scaling theories and simulations have established that various combinations of the bare parameters lead to identical results, provided that the values of X and Y are held fixed. It is clear from eq 17 that the parameters required to carry out an equilibrium BD simulation of a coarse-grained bead−spring chain are $\{N, b, q, l^*_B, l^*_D\}$ (since hydrodynamic interactions do not influence static properties). In the presence of flow, the additional parameters h^* and $\dot{\gamma}^*$ must also be prescribed. For a particular choice of N, the bead−spring chain parameters $\{q, b, l^*_B, l^*_D\}$ are related to the bare parameters through eqs (5), (13), and the expressions $l^*_B = (l_B/b_k)b^*_k$ and $l^*_D = (l_D/b_k)b^*_k$, where the quantity b^*_k is simply obtained by equating the expressions for the chain length in the bare model and in the bead−spring chain model. Thus, $L = N_k b_k = (N-1)Q_0 = (N-1)\sqrt{b}l_H$, which implies, $b^*_k = b_k/l_H = (N-1)\sqrt{b}/N_k$. Note that the choice of the level of coarse-graining N is fundamentally arbitrary. In this work, we wish to examine whether various combinations of bead−spring chain parameters lead to identical results, provided that the values of X, Y, and β (in the presence of flow), are held fixed. Using eqs 1−3, 5, and 13 and the expression for b^*_k, one can show that the scaling variables are related to the bead−spring chain parameters through the expressions

$$X = \left[\frac{N^4 q^4 l^{*2}_B (b+5)}{3(N-1)b}\right]^{1/3}; \; Y = l^*_D\left[\frac{N^2 q^2 l^{*2}_B (b+5)^2}{9(N-1)^2 b^2}\right]^{1/3} = l^*_D\sqrt{\frac{X(b+5)}{3(N-1)b}} \tag{18}$$

It is consequently possible to choose various levels of coarse-graining N, for the same values of X and Y, through a suitable choice of the remaining BD simulation parameters $\{b, q, l^*_B, l^*_D\}$.

Table 1 displays a representative set of values for the bare model parameters, the resultant scaling variables X and Y, and the corresponding values for the bead−spring chain parameters used in the simulations carried out here. Typically, two to three different values of N are used for each value of X. Note that Y can be varied independently of X by just changing (l_D/b_k) (and keeping all other bare model parameters fixed). As a result, the dependence of properties of the polyelectrolyte solution as a function of X and Y can be explored by carrying out BDS, and a rigorous evaluation of the usefulness of the electrostatic blob model can be made.

3. Equilibrium End-to-End Vector

A comprehensive and clear analysis of the various issues involved in the comparison of simulation results for the equilibrium properties of dilute polyelectrolyte solutions with the predictions of scaling theories, has been given in the recent publication of Everaers et al.[4] In order to place the results of our simulations in the context of current scaling theories, we first briefly summarize here the salient features of the discussion by Everaers et al.

As suggested by the phase-diagram displayed in Figure 2, there are broadly two schools of thought with regard to the equilibrium scaling of the conformations of a polyelectrolyte chain in the X and Y parameter space. These have been denoted as KMBJ[7−10] and OSFKK[11−13] by Everaers et al., after the initials of the main authors of these theories. Clearly, there are regions of parameter space in the phase-diagram in which the predictions of the two theories are identical, and regions in which they differ. The common regions are as follows.

Table 1. Representative Sets of Values for the Bare Model Parameters $\{N_k, s, l_B/b_k, l_D/b_k\}$, the Resultant Scaling Variables X and Y, and the Corresponding Values for the Bead−Spring Chain Parameters $\{N, b, q, l_B^*, l_D^*\}$, Used in Brownian Dynamics Simulations[a]

X	$\{N, b, q, l_B^*\}$	$\{N_k, s, l_B/b_k\}$	Y	l_D^*	l_D/b_k	$\eta_{p,0}^*$ (no HI)	$\eta_{p,0}^*$ ($h^* = 0.25$)	$\eta_{p,0}^*$ ($h^* = 0.15$)
	{12, 60.45, 1.67, 0.57}	{240, 12, 1.61}	0.05	0.08	0.221			
12	{16, 55.80, 1.19, 0.74}	{304, 16, 2.01}	1.00	1.86	5.03			
	{20, 58.16, 1.00, 0.75}	{400, 20, 2.08}	16.00	33.46	92.38			
	{16, 91.00, 1.88, 0.46}	{480, 16, 1.56}	0.05	0.08	0.27	80.88 ± 0.86	54.66 ± 1.35	60.19 ± 2.12
	{16, 91.00, 1.88, 0.46}	{480, 16, 1.56}	1.00	1.63	5.48	213.02 ± 1.74	145.65 ± 2.33	170.81 ± 4.12
	{16, 91.00, 1.88, 0.46}	{480, 16, 1.56}	16.00	26.12	87.63	446.33 ± 2.23	291.23 ± 2.24	
	{20, 89.74, 1.50, 0.52}	{600, 20, 1.74}	0.05	0.09	0.31	126.06 ± 3.49	76.14 ± 1.67	
16	{20, 89.74, 1.50, 0.52}	{600, 20, 1.74}	1.00	1.84	6.12	342.73 ± 5.9	220.94 ± 3.04	
	{20, 89.74, 1.50, 0.52}	{600, 20, 1.74}	16.00	29.39	97.98	706.66 ± 2.78	366.64 ± 3.42	
	{24, 57.61, 1.67, 0.32}	{480, 12, 0.88}	0.05	0.1	0.27		97.53 ± 2.30	
	{24, 57.61, 1.67, 0.32}	{480, 12, 0.88}	1	1.99	5.48		285.28 ± 2.76	
	{24, 47.17, 1.67, 0.32}	{400, 10, 0.80}	16.00	31.59	80.00			
	{20, 89.74, 1.50, 0.73}	{600, 20, 2.43}	0.05	0.08	0.27			
20	{24, 47.17, 1.67, 0.44}	{400, 10, 1.12}	1.00	1.77	4.47			
	{26, 91.00, 1.54, 0.47}	{800, 20, 1.58}	16.00	30.17	101.19			
	{24, 99.35, 3.33, 0.15}	{800, 10, 0.52}	0.05	0.08	0.29		104.78 ± 2.37	
	{24, 99.35, 3.33, 0.15}	{800, 10, 0.52}	1	1.65	5.77		335.81 ± 2.3	
24	{28, 61.67, 1.79, 0.41}	{600, 12, 1.15}	1.00	1.77	5.00			
	{32, 72.42, 1.25, 0.69}	{800, 20, 2.08}	16.00	30.46	92.38			

[a] Values in the last three columns (where displayed), are the zero-shear rate viscosity $\eta_{p,0}^*$ obtained from equilibrium simulations, using eq 20 in the absence of HI, and a Green−Kubo expression in the presence of HI.[25,47]

1. $1 < X < \infty$ and $Y \rightarrow \infty$. In the absence of screening, the monomers interact through an infinite range Coulomb potential, and the chains are stretched into a *blob pole*

$$\frac{\langle r^2 \rangle}{\xi^2} \simeq X^2$$

2. $0 < Y < \infty$ and $X \rightarrow \infty$. For chains that are sufficiently long, the Debye−Hückel screened electrostatic interaction potential is effectively short-ranged, and leads to a self-avoiding-walk (SAW) behavior

$$\frac{\langle r^2 \rangle}{\xi^2} \simeq X^{2\nu}$$

where ν is the Flory exponent.

3. $Y \ll 1$. When the screening is strong, the electrostatic interaction potential reduces to a simple excluded volume potential. A Flory type argument balancing the pairwise electrostatic repulsion between monomers, with the entropic elasticity of a Gaussian chain, leads to

$$\frac{\langle r^2 \rangle}{\xi^2} \simeq \begin{Bmatrix} X & \text{for } X < Y^{-4} \\ Y^{4/5}X^{6/5} & \text{for } X > Y^{-4} \end{Bmatrix}$$

The main difference between the two theoretical approaches is related to the conditions under which the blob pole crosses over to the SAW regime. This is directly linked to the question of whether the electrostatic persistence length l_{el} scales as l_D according to KMBJ, or l_D^2 according to OSFKK. Basically, while it is agreed that the chain first bends when $X \sim (l_{el}/\xi)$, the controversy arises in the estimation of l_{el}. As shown in Figure 2, there is a direct crossover in the KMBJ picture from the blob pole to the SAW regime for $X > Y$, while in the OSFKK picture, the phase diagram is much more complex, with a regime between the blob pole and the SAW regime, and the crossover occurring for $X > Y^2$.

Everaers et al.[4] have carefully examined the validity of the two scaling theories by carrying out extensive Monte Carlo simulations. They conclude, with the help of a scaling plot similar to that displayed in Figure 2, that the KMBJ picture is false, and show that verifying the veracity of the OSFKK scaling picture requires simulation of chains with astronomical chain lengths. They argue that, as a result, though different exponents are predicted by these theories, the absolute differences between observables for typically simulated chain lengths, are small.

Since this is a preliminary study examining whether the results of BDS can be represented in terms of scaling variables, we have not attempted to resolve the fine details of the asymptotic behavior of observables between various crossover lines. In this spirit, Figure 3a displays the variation of $\langle r^2 \rangle/\xi^2$ with Y, for various values of X. It is immediately apparent that different data sets overlap when rescaled to the definition of the electrostatic blob. Thus, for three different levels of coarse-graining, the predicted behavior of $\langle r^2 \rangle/\xi^2$ is identical, provided X and Y are the same. It is intuitively clear that in order to maintain the integrity of the conformation of the blob chain, a choice of $N \geq X$ must be made. This is indeed the case, as shown in Figure 3b, where as Y increases, data for $N = 10$ does not overlap with other data sets for $X = 24$.

Each curve in Figure 3a can be considered to be the variation of $\langle r^2 \rangle/\xi^2$ along a vertical line drawn at a fixed value of X in the phase diagrams shown in Figure 2. From the different scaling regimes in Figure 2, one can anticipate that there will be two regions in which $\langle r^2 \rangle/\xi^2$ will not depend on Y, namely, the limits of small and large Y, where the blob chain is an ideal chain and a rigid rod, respectively. This is clearly reproduced in Figure 3a, with $\langle r^2 \rangle/\xi^2$ independent of Y for $Y \leq 0.1$, and for $Y \geq 10$. At intermediate values of Y, $\langle r^2 \rangle/\xi^2$ is a function of Y. If the dependence on Y is expressed as a power law, $\langle r^2 \rangle/\xi^2 \sim Y^p$ (which appears to be valid for a wide range of intermediate values), then the value of p can be found from the slope of the tangent to the curves at $Y = 1$. Both scaling theories predict that $p = 0.8$ for $Y \sim \mathcal{O}(1)$. The inset to Figure 3a shows that this prediction is captured by BD simulations, with p asymptotically tending to 0.8 for $X \gg 1$. Note that, for the chain lengths simulated here, the OSFKK prediction of an increase in the magnitude of the exponent p to values beyond 0.8 (namely, 6/5 and 2), with increasing values of Y, before a crossover to the region independent of Y, is not observed.

If the dependence of the nondimensional end-to-end vector on the number of blobs is expressed as a power law, $\langle r^2 \rangle/\xi^2 \sim$

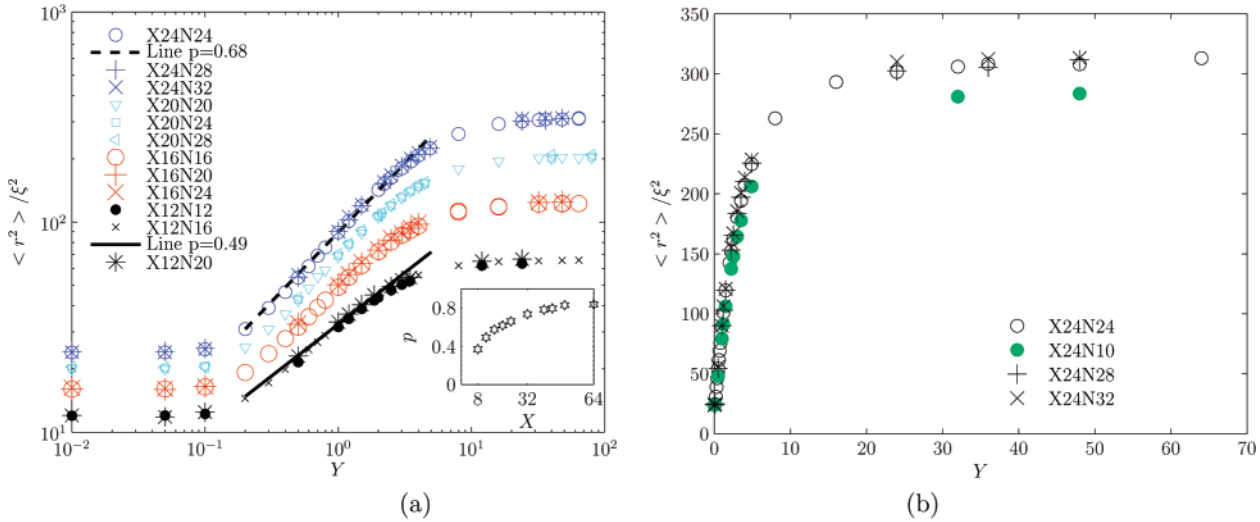

Figure 3. (a) Variation of the nondimensional end-to-end vector $\langle r^2\rangle/\xi^2$ with the reduced screening length Y, for different values of the number of blobs *X*. Three different values of *N* have been used for each value of *X* to demonstrate the parameter free nature of the predictions. The inset shows the dependence of *p* on *X*, where *p* is the exponent in the power law, $\langle r^2\rangle/\xi^2 \sim Y^p$, valid for intermediate values of *Y*. (b) Data collapse does not occur when the level of coarse-graining is coarser than the blob structure, i.e., $N < X$.

X^k, then it is clear from the phase-diagram in Figure 2, that for both scaling theories, $k = 2$ for $Y \rightarrow \infty$ (blob pole regime), and $k = 1$ for $Y \rightarrow 0$ (ideal blob chain regime). However, for intermediate values of *Y*, while the KMBJ picture predicts a unique exponent $k = 1.2$ (SAW regime), the OSFKK theory predicts an additional region between the blob pole and SAW regimes, in which the blob chain behaves ideally.

The exponent *k* predicted by BD simulations is reported in Figure 4, with the shade of color used to represent the magnitude of *k*, as indicated by the color bar on the figure right. The value of *k* has been obtained by carrying out a series of simulations at various fixed values of *Y*, represented by the square symbols on the figure. Basically, simulation data for $\ln\langle r^2\rangle/\xi^2$ vs $\ln X$ was fitted by a polynomial curve, and the value of *k* at any value of *X* was estimated from the slope of the curve at that value of *X*.

Four lines have been drawn in Figure 4 to demarcate important regions in the phase-diagram. The upper most cyan line is the crossover line from $k = 2$ to $k = 1.2$, predicted by the KMBJ theory. The dashed red and dot-dashed pink lines are the crossover lines from $k = 2$ to $k = 1$, and, $k = 1$ to $k = 1.2$, respectively, predicted by the OSFKK theory. Finally, the lower most dotted blue line is the crossover line from $k = 1.2$ to $k = 1$, predicted by both the scaling theories.

There are several conclusions that can immediately be drawn from Figure 4. First, the blob pole and the ideal blob chain regimes are clearly evident for $Y \rightarrow \infty$, and $Y \rightarrow 0$, respectively. Second, the blob pole does not begin to bend along the cyan line, which is the result expected by KMBJ theory. The absence of a crossover has also been observed earlier by Everaers et al.[4] in their Monte Carlo simulations, and has been used by them to demonstrate the inaccuracy of KMBJ theory. Third, the ideal chain regime expected by OSFKK theory between the blob pole and SAW regimes (i.e., between the dashed red and dot-dashed pink lines) is not evident in the BD simulations. Indeed, while the dashed red line seems roughly to coincide with a change in the exponent *k*, the entire region between the dashed red and dotted blue lines (and even beyond to lower values of *Y*), appears to be a smooth crossover between the blob pole and ideal blob chain regimes. There does not appear to be a sharply defined regime where $k = 1.2$. Finally, the onset of the ideal blob chain regime seems to begin for $Y \lesssim 0.2$, which is smaller than the range of values expected by OSFKK theory (indicated by the dotted blue line). Two points, however, are perhaps worth noting. The values of *X*, and consequently chain lengths, explored here are very small, and it should not be surprising that asymptotic scaling behavior is not observed. Further, scaling theories do not account for numerical prefactors, and as a result, the absolute position of crossover lines on the phase-diagram should not be expected to be accurate. The key fact, however, that emerges from Figure 4, is that BD simulations can be used to construct a phase-diagram in the *X* and *Y* parameter space, and in principle (though perhaps not easily in practice), exact demarcations of the various regimes can be obtained by carrying out simulations with much longer bead−spring chains than those used here.

It should be noted that when the screening length is large compared to the size of the chain, and the chain is in the strongly stretched regime, the assumption of both scaling theories that the blob size is uniform along the length of the chain is no longer valid. This nonuniformity gives rise to a logarithmic correction to the prediction by scaling theories of a linear dependence of the end-to-end vector on the number of blobs. However, in all the simulations carried out in our work (both equilibrium and flow), we have not explored the regime $Y \gg X$ where the logarithmic corrections might be expected to be large enough to become significant. The collapse of the static data onto the predictions of scaling theory and (as will be demonstrated shortly), the adequacy of the scaling variables to describe the shear flow data, appears to support this conclusion.

The great advantage of Brownian dynamics simulations is that the behavior of dilute polyelectrolyte solutions can be predicted both at equilibrium and far from equilibrium, within the same consistent framework. In the section below, we examine the shear rate dependence of the end-to-end vector, the viscosity and the first normal stress difference of dilute polyelectrolyte solutions, with equilibrium polyelectrolyte chain conformations drawn from different conformational regions in the phase diagram. The values of *X* and *Y* that correspond to these chosen conformational states have been indicated in Figure 4 by the filled squares.

4. Shear Flow

Pamies et al.[30] have recently used Brownian dynamics simulations of a charged bead−spring chain model, with screened Debye−Hückel electrostatic interactions between the

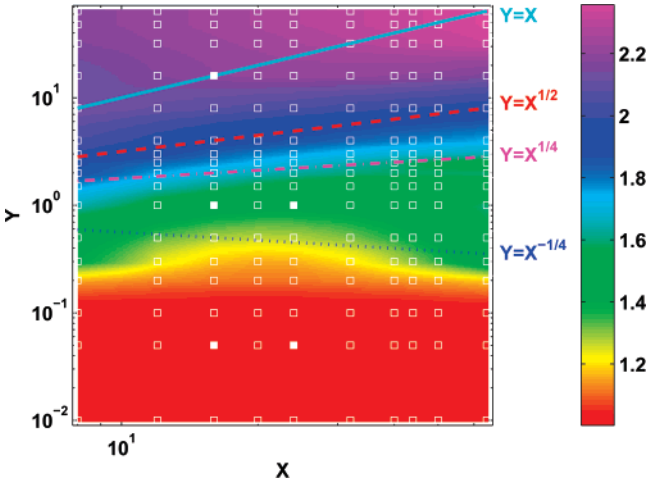

Figure 4. Variation of k in the X and Y parameter space, where k is the exponent in the power law, $\langle r^2\rangle/\xi^2 \sim X^k$. The magnitude of k is represented by the shade of color and can be estimated from the color bar on the figure right. The various lines are crossover lines demarcating different regions in the phase-diagram, predicted by the KMBJ and OSFKK theories (see Figure 2). The empty square symbols indicate the values of X and Y used in the simulations to find k, and the filled squares represent the points in the phase-diagram used in the shear flow simulations.

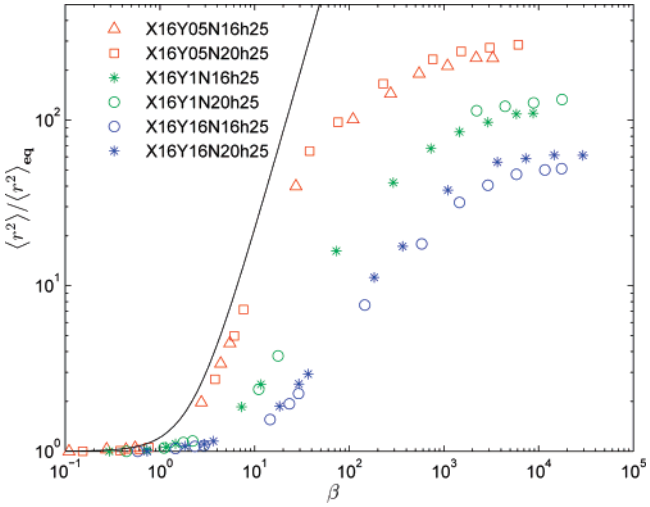

Figure 5. Dependence of the size ratio $\langle r^2\rangle/\langle r^2\rangle_{eq}$ on the characteristic shear rate β, for $X = 16$, at three different values of the reduced screening length, $Y = 0.05$, $Y = 1$, and $Y = 16$. The hydrodynamic interaction parameter $h^* = 0.25$. Symbol colors reflect the location of X and Y in the conformational phase space of Figure 4. The black curve is the prediction of the Rouse theory (see eq 19).[27] Two different values of the number of beads, $N = 16$ and $N = 20$, have been studied for each value of Y.

beads, to predict the behavior of dilute polyelectrolyte solutions undergoing shear flow. They have examined the influence of both the screening length, and the charge density, on the radius of gyration and the intrinsic viscosity of the solution. By choosing appropriate values for these parameters, they have been able to identify coillike and rodlike configurations of the chains and, as a result, study the different responses in shear flow which arise due to differences in the initial conformational states. The influence of hydrodynamic interactions on the predicted shear rate dependence of the viscosity, and the relevance of the initial conformational state in this context, has also been examined by them. As mentioned earlier, however, the number of beads N in their model, remains an arbitrary parameter. While the results presented in this section are qualitatively similar to the results of Pamies et al.,[30] we have attempted to interpret the data in the light of the scaling theories discussed in the sections above.

The growth of the size ratio $\langle r^2\rangle/\langle r^2\rangle_{eq}$ vs the characteristic shear rate β, is displayed in Figure 5 at three different values of the reduced screening length, $Y = 0.05$, $Y = 1$, and $Y = 16$. These three values of Y correspond to the ideal blob chain, the SAW-like blob chain, and the blob pole regimes, respectively, with the symbol colors in Figure 5 reflecting the location of the pair (X, Y) in the conformational phase space of Figure 4. Two different values of N have been used for each value of Y. The plot clearly indicates that, as was observed previously in the case of equilibrium simulations for the nondimensional end-to-end vector, the data collapses onto master curves, independently of the bare model and bead−spring chain parameters, provided the scaling variables are identical. The dependence of the rate of chain unraveling on the location of the equilibrium conformation of the chain in the static phase diagram is evident. For the purpose of comparison, the black curve in the figure is the analytical result for Rouse chains[27]

$$\frac{\langle r^2\rangle}{\langle r^2\rangle_{eq}} = 1 + \frac{1}{5}\frac{N(N^2+1)}{(N-1)^2(N+1)}\beta^2 \qquad (19)$$

which has been drawn in the figure for $N = 20$. In the Rouse case, the end-to-end vector does not level off and saturate to a maximum value since the springs in the model are infinitely extensible. Further, note that the N dependence disappears in the limit of large N, leading to a universal prediction of a quadratic dependence of the end-to-end vector ratio on β. As might be anticipated, of the three equilibrium static conformations of the polyelectrolyte chain, the conformation drawn from the regime where the chain is an ideal blob chain comes closest to the Rouse curve. Since electrostatic interactions are highly screened, the difference from the Rouse curve arises for two reasons. First, the presence of hydrodynamic interactions appears to slow down the unraveling of the chain, and second, the presence of finite extensibility leads to the stretch of the end-to-end vector leveling off at high shear rates. These features have been observed previously for uncharged polymers.[48] As the electrostatic interactions become less screened with increasing Y, both the rate at which the chain is stretched, and the ultimate saturation value at high shear rates is significantly decreased. These differences in the curves are correlated to the fact that the displayed data is in terms of the end-to-end vector $\langle r^2\rangle$ divided by $\langle r^2\rangle_{eq}$, the latter of which increases with increasing Y, as can be seen from Figure 3a.

The dependence of the nondimensional polymer contribution to viscosity, defined by $\eta_p^* = \eta_p/\lambda_H n_p k_B T$, on the nondimensional shear rate $\dot\gamma^* = \lambda_H\dot\gamma$, for $X = 16$, is displayed in Figure 6, at three different values of the reduced screening length, Y. Both free-draining and fluctuating HI cases have been examined. It is clear from the figure that the viscosity at low shear rates gets larger as the configuration of the chain becomes more extended, due to the longer range of the electrostatic interactions with increasing Y. In the Rouse theory, where only the connectivity between beads through Hookean springs is taken into account, and no other intrachain interactions are incorporated, shear thinning is not predicted.[27] The inclusion of any or all of the nonlinear phenomena of FENE springs, excluded volume effects and hydrodynamic interactions leads to a shear rate dependence of viscosity.[22] It is clear from Figure 6 that shear thinning is also predicted in the presence of electrostatic interactions, with a complex dependence that is influenced both by the conformational state at equilibrium, and the presence or absence of HI. The incorporation of HI evidently leads to a reduction in the predicted value of viscosity. The extent of this

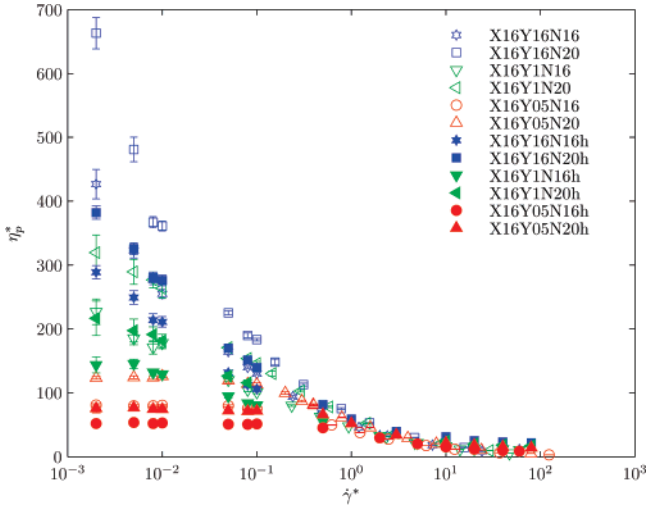

Figure 6. Dependence of the nondimensional polymer contribution to viscosity η_p^* on the nondimensional shear rate $\dot{\gamma}^*$, for $X = 16$, at three different values of the reduced screening length, $Y = 0.05$, $Y = 1$, and $Y = 16$. Symbol colors reflect the location of X and Y in the conformational phase space of Figure 4. Filled symbols correspond to simulations with hydrodynamic interactions incorporated, while empty symbols represent free-draining simulations. Two different values of the number of beads, $N = 16$ and $N = 20$, have been studied for each value of Y.

reduction decreases as the shear rate increases and the chains become more extended, with a concomitant weakening of hydrodynamic interactions. Note that all simulations with HI reported in Figures 5−7 have been carried out with $h^* = 0.25$. This is the value commonly used in simulations of dilute solutions of uncharged polymers.[14] The plateau in the viscosity as a function of shear rate, which is observed for the ideal blob chain configuration ($Y = 0.05$) at low shear rates, disappears as the chain approaches the blob pole ($Y = 16$) regime. In the latter case, shear thinning is already present at the lowest shear rate examined here, which is characteristic of solutions of rigid rods. All these qualitative observations have been noted earlier by Pamies et al.[30] In particular, the dependence of the predictions on the choice of the degree of coarse-graining N observed in Figure 6, is also clearly evident in the simulations reported by them.

A different perspective is obtained when the viscosity is scaled with the zero-shear-rate viscosity $\eta_{p,0}$, and the shear rate is scaled with the characteristic relaxation time λ_p. Note that evaluation of λ_p also requires $\eta_{p,0}$, since one can show that for dilute polymer solutions, $\lambda_p = \eta_{p,0}/n_p k_B T$. In the absence of HI, the zero-shear-rate viscosity has been obtained from the expression,[49]

$$\eta_{p,0}^* = \frac{2}{3} N \langle R_g^{*2} \rangle \tag{20}$$

where $\langle R_g^{*2} \rangle$ is the nondimensional mean square radius of gyration at equilibrium. In the presence of HI, $\eta_{p,0}^*$ has been calculated by using a Green-Kubo expression for the autocorrelation function of the shear stress, obtained from equilibrium simulations.[25,47] The values of $\eta_{p,0}^*$ obtained using these two procedures, for the various cases studied here, are listed in the last two columns of Table 1. Plots of the relative viscosity $\eta_p^*/\eta_{p,0}^*$ vs the characteristic shear rate β are displayed in Figure 7, parts a−c, for blob chains with $X = 16$ blobs, at three different values of Y, using at least two values of N for each of these values of Y. As in Figures 5 and 6, symbol colors reflect the location of X and Y in Figure 4.

Figure 7a, representing free-draining simulations, shows a complete collapse of data at different values of N, when represented in terms of blob model scaling variables. A clear difference in behavior between the different equilibrium polymer conformations, in terms of the onset and rate of shear thinning, is readily apparent across the entire range of shear rates examined here. At high shear rates, the different curves come together as finite extensibility becomes the dominant effect, and electrostatic interactions are weakened. Data collapse for different values of N is also observed for simulations with HI in Figure 7b. Note that the difference between the SAW and blob pole regimes is not as large as in the case of free-draining simulations. This is also visible in Figure 7c, where when simulations with and without HI are compared, it is interesting to see that the role of HI is less significant for the SAW-like configuration ($Y = 1$) compared to the ideal blob chain ($Y = 0.05$) and rodlike configurations ($Y = 16$). Pamies et al.[30] have pointed out earlier that HI is less significant for rodlike configurations relative to coillike configurations. Another difference between free-draining simulations and simulations with HI is revealed at high shear rates. While the free-draining viscosity for ideal blob chains with $Y = 0.05$ decreases continuously until its value is equal to the viscosity in the other two more extended regimes, the rate of shear thinning appears to slow down at high shear rates in the presence of HI, with the viscosity not yet equal to that of the other configurations at a characteristic shear rate of 10^4.

Interesting insights can be obtained when the dependence of the relative viscosity and the first normal stress difference coefficient on the characteristic shear rate β, is displayed in a log−log plot, as in Figure 8. As can be seen from the figures, there appear to be atleast two or three distinct regimes in the dependence of the viscometric functions on the reduced shear rate, depending on the value of Y. In both the cases examined, a Newtonian regime of constant viscosity or first normal stress difference coefficient is observed, followed by shear thinning regimes where the relative viscosity and the first normal stress difference coefficient obey a power-law dependence on shear rate, β^{-m}. For a SAW-like blob chain, two power-law shear thinning regimes are observed, while for an ideal blob chain, only a single power-law regime of shear thinning is observed. In each of the shear thinning regimes, the power-law exponent for the first normal stress difference coefficient is roughly twice the exponent for the viscosity ratio. Previous studies of the power law exponent describing shear thinning of the relative viscosity due to FENE effects have reported values in the region of 0.5−0.6 for m.[50−52] The power-law exponent of $m = 0.56$ observed for $Y = 0.05$ in Figure 8a suggests that the ideal blob chain undergoes a crossover directly from the Newtonian regime into the shear thinning regime where finite extensibility effects dominate. On the other hand, a SAW-like blob chain initially experiences a slower degree of shear thinning before a crossover into the FENE dominated regime. As was observed in Figures 7, hydrodynamic interactions are weak for a SAW-like blob chain, and as a result, electrostatic interactions may be expected to be the dominant mechanism responsible for this intermediate shear thinning regime. Using renormalization group methods, Öttinger[53] has previously found that the values, $m = 0.25$ and $m = 0.5$, describe the power law shear rate dependence of $\eta_p/\eta_{p,0}$, and $\Psi_1/\Psi_{1,0}$, respectively, for uncharged chains in the excluded volume limit. These predictions were subsequently corroborated in the long chain limit by Brownian dynamics simulations of Rouse chains with excluded volume interactions carried out in our group.[54] The values of 0.23 and 0.55 observed

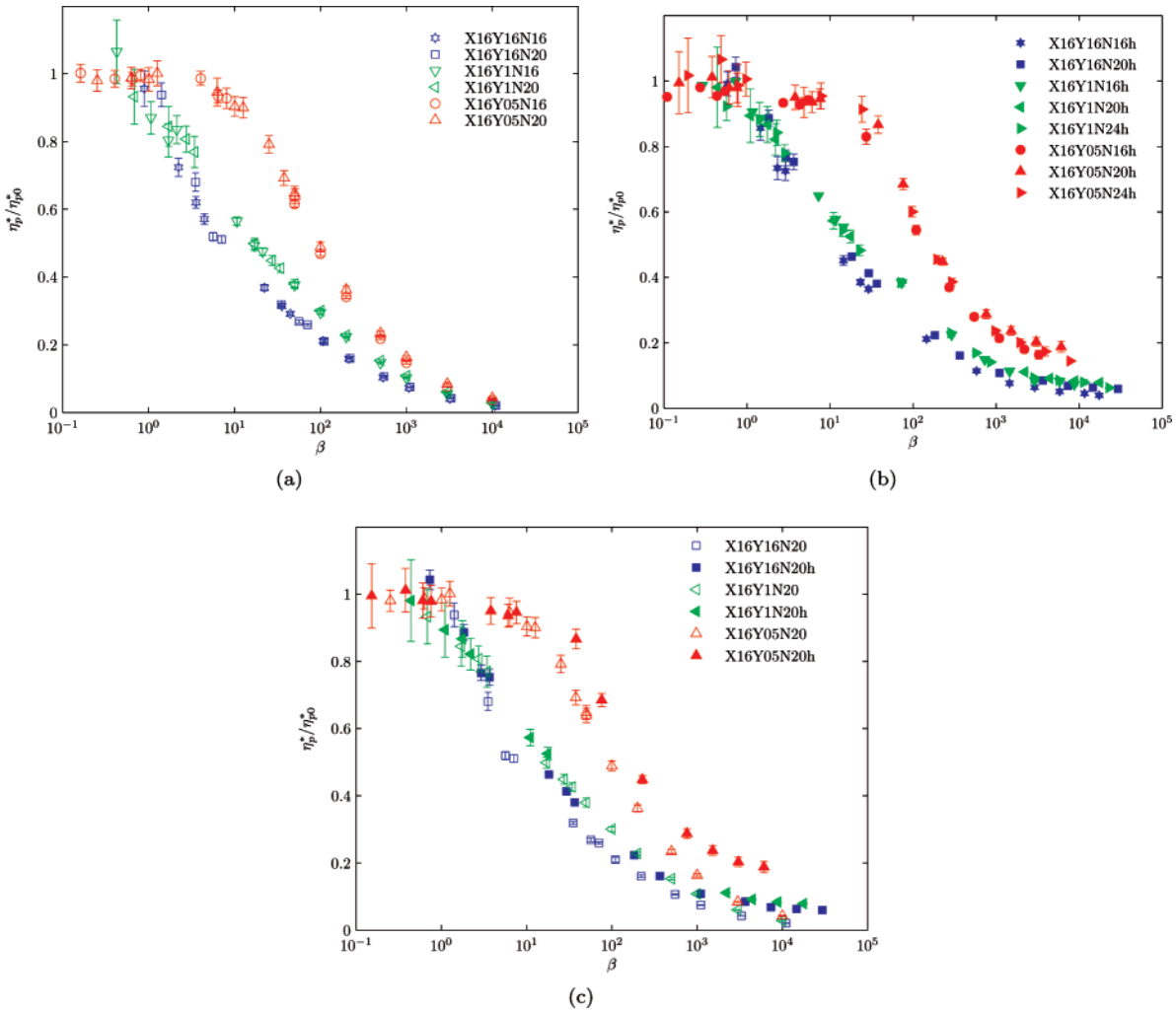

Figure 7. Relative viscosity vs the characteristic shear rate, for $X = 16$ blobs, at three different values of the reduced screening length, $Y = 0.05$, $Y = 1$, and $Y = 16$. Two values of $N = 16$ and $N = 20$ have been examined for each value of Y. Symbol conventions are as in Figure 6. Key: (a) free-draining simulations; (b) simulations with HI present; (c) comparison of free-draining and HI results.

for m in Figure 8a and Figure 8b, for the nondimensional screening length $Y = 1$, clearly suggests, perhaps not surprisingly, that screened electrostatic interactions give rise to an intermediate shear thinning behavior which is analogous to that for chains with excluded volume interactions. At very high shear rates, the symbols representing BDS data can be seen to level off and depart from the straight lines representing power-law shear thinning behavior. As can be seen from Figure 5, these shear rates correspond to the regime where the chains are no longer being extended by the shear flow, and are approaching their saturation value of stretch.

The dependence of the viscometric functions on the number of blobs, and the influence of the choice of value for the hydrodynamic interaction parameter h^* has also been examined in Figure 8. Interestingly, when represented in terms of scaling variables, the shear rate dependence of these properties seems to be relatively insensitive to the length of the blob chain, and appears to only strongly depend on the regime in conformational space occupied by the equilibrium configuration of the chain. Further simulations for a larger range of values of X are necessary to explore the extent of this insensitivity.

A question that arises in simulations that include hydrodynamic interactions is the proper choice of value for the hydrodynamic interaction parameter h^*. An important result in the theory of hydrodynamic interactions in dilute solutions of flexible homopolymers is that this choice becomes irrelevant in the "nondraining" limit $h \rightarrow \infty$, where h, the so-called "draining" parameter, defined by $h = h^*\sqrt{N}$, is a measure of the strength of hydrodynamic interactions. Further, it has been shown that choosing the "fixed-point" value for h^* ($h^* = 0.25$), leads to predictions in the nondraining limit for relatively small values of chain length N. (For a recent discussion of these results in the context of BDS, and the relevant references, see ref 24.) This latter result is the motivation behind the frequent use of $h^* = 0.25$ in many of the BD simulations reported in the literature. To our knowledge, the value of the fixed-point for h^* in the presence of electrostatic interactions has not yet been established. In order to examine whether the simulations results reported here can be considered to be in the nondraining limit, we have carried out simulations for two different values of h^*, namely, 0.25 and 0.15. As can be seen clearly from the results displayed in Figure 8, the choice of h^* appears to have no effect on the dependence of the viscometric functions on the characteristic shear rate. This indicates that the chain lengths considered here appear to be sufficient to attain the nondraining limit.

The collapse of data observed in Figure 8 strongly suggests that a master plot for the dependence of viscometric functions on characteristic shear rate can be constructed, once and for all, for a wide range of values of reduced screening length Y, independent of the choice of parameter values in the bead−spring chain model.

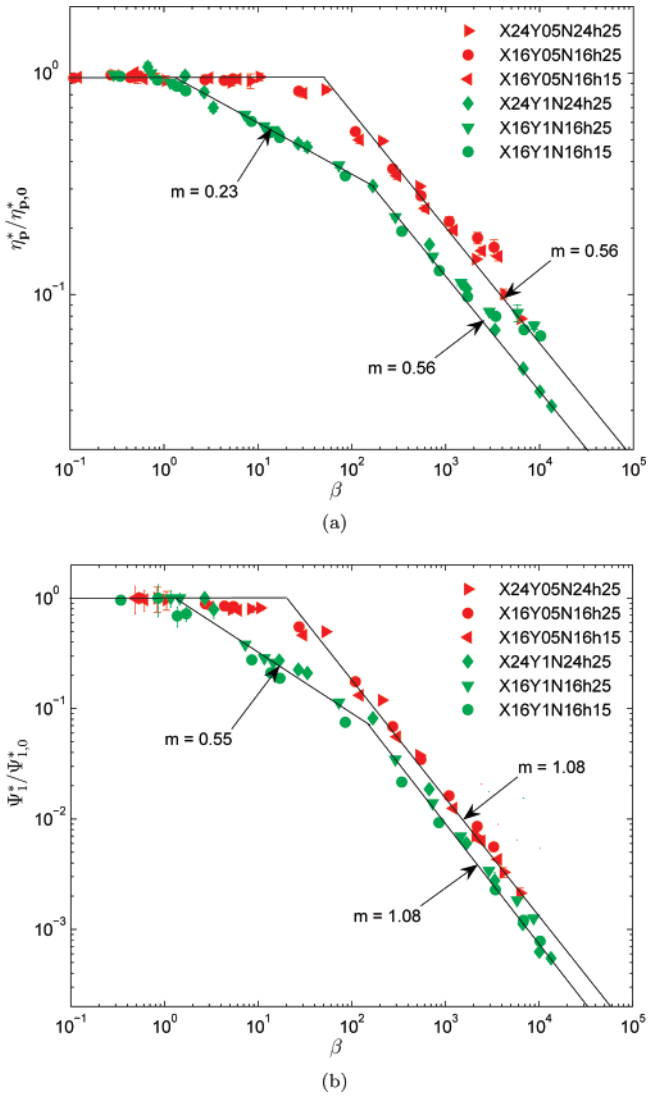

Figure 8. (a) Relative viscosity and (b) first normal stress difference coefficient, vs the characteristic shear rate, for $X = 16$ and $X = 24$, at two different values of the reduced screening length, $Y = 0.05$ and $Y = 1$, and at two different values of the hydrodynamic interaction parameter, $h^* = 0.15$ and $h^* = 0.25$. Symbol conventions are as in Figure 7.

5. Conclusions

A bead−spring chain model, in which the beads are charged and interact with each other through a screened Debye−Hückel potential, has been used to examine the rheological behavior of dilute polyelectrolyte solutions. The equilibrium electrostatic blob model of de Gennes et al.[3] has been used to provide the framework within which the results of Brownian dynamics simulations can be interpreted. The most important conclusions of this study are as follows: (i) equilibrium results for the nondimensional end-to-end vector $\langle r^2\rangle/\xi^2$ can be completely collapsed onto a master plot when viewed as a function of the number of blobs X and the reduced screening length Y (see Figure 3), and (ii) with the inclusion of the characteristic shear rate β as the additional scaling variable, a parameter free prediction of the dependence on β of the size ratio $\langle r^2\rangle/\langle r^2\rangle_{eq}$, of the relative viscosity $\eta_p^*/\eta_{p,0}^*$, and of the first normal stress difference coefficients ratio $\Psi_1^*/\Psi_{1,0}^*$, can be obtained, independent of the choice of parameters in the bead−spring chain model (see Figures 5 and 8).

While it has been shown in this work that a mere knowledge of the location of the chain in the static phase diagram is already sufficient to enable a parameter free comparison of experimental data and theoretical predictions, it would be interesting to examine the continued validity of the electrostatic blob model away from equilibrium, in a flow situation, and establish the connection to a deformed Pincus blob.[34,35] The recent paper by Colby and co-workers[33] gives powerful insight into how the blob picture might continue to be valid even in the presence of flow. An additional tool in this regard would be to carry out a detailed chain mode analysis in the presence of flow. We hope to analyze Brownian dynamics simulations data along these lines in our future work.

References and Notes

(1) Barrat, J. L.; Joanny, J. F. *Adv. Chem. Phys.* **1996**, *XCIV*, 1−66.
(2) Ullner, M. Polyelectrolyte models in theory and simulation. In *Handbook of polyelectrolytes and their applications*; Tripathy, S. K., Kumar, J., Nalwa, H. S., Eds.; American Scientific Publishers: Stevenson Ranch, CA, 2002; Vol. 3.
(3) de Gennes, P. G.; Pincus, P.; Velasco, R. M.; Brochard, F. *J. Phys. (Paris)* **1976**, *37*, 1461−1473.
(4) Everaers, R.; Milchev, A.; Yamakov, V. *Eur. Phys. J. E* **2002**, *8*, 3−14.
(5) Dobrynin, A. V.; Rubinstein, M. *Prog. Polym. Sci.* **2005**, *30*, 1049−1118.
(6) De Gennes, P.-G. *Scaling Concepts in Polymer Physics*; Cornell University Press: Ithaca, NY, 1979.
(7) Kuhn, W.; Kunzle, O.; Katchalsky, A. *Helv. Chim. Acta* **1948**, *31*, 1994−2037.
(8) Muthukumar, M. *J. Chem. Phys.* **1996**, *105*, 5183−5199.
(9) Ghosh, K.; Carri, G. A.; Muthukumar, M. *J. Chem. Phys.* **2001**, *115*, 4367−4375.
(10) Barrat, J. L.; Joanny, J. F. *Europhys. Lett.* **1993**, *24*, 333−338.
(11) Khokhlov, A. R.; Khachaturian, K. A. *Polymer* **1982**, *23*, 1742−1750.
(12) Odijk, T. *J. Polym. Sci., Polym. Phys. Ed.* **1977**, *15*, 477−483.
(13) Skolnick, J.; Fixman, M. *Macromolecules* **1977**, *10*, 944−948.
(14) Larson, R. G. *J. Rheol.* **2004**, *49*, 1−70.
(15) Shaqfeh, E. S. G. *J. Non-Newtonian Fluid Mech.* **2005**, *130*, 1−28.
(16) Bird, R. B.; Öttinger, H. C. *Annu. Rev. Phys. Chem.* **1992**, *43*, 371−406.
(17) Prakash, J. R. The kinetic theory of dilute solutions of flexible polymers: Hydrodynamic interaction. In *Advances in flow and rheology of non-Newtonian fluids*; Siginer, D. A., Kee, D. D., Chhabra, R. P., Eds.; Elsevier Science: Rheology Series; Elsevier: Amsterdam, 1999.
(18) Prabhakar, R.; Prakash, J. R. *J. Rheol.* **2006**, *50*, 561−593.
(19) Öttinger, H. C. *Stochastic Processes in Polymeric Fluids;* Springer-Verlag: Berlin, 1996.
(20) Jendrejack, R. M.; de Pablo, J. J.; Graham, M. D. *J. Chem. Phys.* **2002**, *116*, 7752−7759.
(21) Hsieh, C.-C.; Li, L.; Larson, R. G. *J. Non-Newtonian Fluid Mech.* **2003**, *113*, 147−191.
(22) Prabhakar, R.; Prakash, J. R. *J. Non-Newtonian Fluid Mech.* **2004**, *116*, 163−182.
(23) Prabhakar, R.; Prakash, J. R.; Sridhar, T. *J. Rheol.* **2004**, *48*, 1251−1278.
(24) Sunthar, P.; Prakash, J. R. *Macromolecules* **2005**, *38*, 617−640.
(25) Sunthar, P.; Nguyen, D. A.; Dubbelboer, R.; Prakash, J. R.; Sridhar, T. *Macromolecules* **2005**, *38*, 10200−10209.
(26) Pamies, R.; Martinez, M. C. L.; Hernandez Cifre, J. G.; Garcia de la Torre, J. *Macromolecules* **2005**, *38*, 1371−1377.
(27) Bird, R. B.; Curtiss, C. F.; Armstrong, R. C.; Hassager, O. *Dynamics of Polymeric Liquids - Volume 2: Kinetic Theory*, 2nd ed.; John Wiley: New York, 1987.
(28) Dunlap, P. N.; Leal, L. G. *Rheol. Acta* **1984**, *23*, 238−249.
(29) Andrews, N. C.; McHugh, A. J.; Schieber, J. D. *J. Polym. Sci., Polym. Phys. Ed.* **1998**, *36*, 1401−1417.
(30) Pamies, R.; Cifre, J. H.; Torre, J. G. D. L. *J. Polym. Sci., Polym. Phys. Ed.* **2007**, *45*, 1−9.
(31) Pamies, R.; Hernandez Cifre, J. G.; De la Torre, J. G. *J. Polym. Sci., Polym. Phys. Ed.* **2007**, *45*, 714−722.
(32) Borisov, O. V.; Darinskii, A. A.; Zhulina, E. B. *Macromolecules* **1995**, *28*, 7180−7187.
(33) Colby, R. H.; Boris, D. C.; Krause, W. E.; Dou, S. *Rheol. Acta* **2007**, *46*, 569−575.
(34) Pincus, P. *Macromolecules* **1976**, *9*, 386−388.
(35) Rubinstein, M.; Colby, R. H. *Polymer physics;* Oxford University Press: London, 2003.
(36) Underhill, P. T.; Doyle, P. S. *J. Non-Newtonian Fluid Mech.* **2004**, *122*, 3−31.
(37) Sunthar, P.; Prakash, J. R. *Europhys. Lett.* **2006**, *75*, 77−83.

(38) Pham, T. T.; Sunthar, P.; Prakash, J. R. *J. Non-Newtonian Fluid Mech.* **2007**, in press (doi:10.1016/j.jnnfm.2007.05.01231).
(39) Schäfer, L. *Excluded Volume Effects in Polymer Solutions;* Springer-Verlag: Berlin, 1999.
(40) Doi, M.; Edwards, S. F. *The Theory of Polymer Dynamics;* Oxford University Press: New York, 1986.
(41) Bird, R. B.; Armstrong, R. C.; Hassager, O. *Dynamics of Polymeric Liquids - Volume 1: Fluid Mechanics,* 2nd ed.; John Wiley: New York, 1987.
(42) Rotne, J.; Prager, S. *J. Chem. Phys.* **1969**, *50*, 4831−4837.
(43) Jendrejack, R. M.; Graham, M. D.; de Pablo, J. J. *J. Chem. Phys.* **2000**, *113*, 2894−2900.
(44) Fixman, M. *Macromolecules* **1986**, *19*, 1204−1207.
(45) Wagner, N. J.; Öttinger, H. C. *J. Rheol.* **1997**, *41*, 757−768.
(46) Prakash, J. R. *J. Rheol.* **2002**, *46*, 1353−1380.
(47) Prabhakar, R.; Prakash, J. R. *J. Rheol.* **2002**, *46*, 1191−1220.
(48) Prabhakar, R. Predicting the rheological properties of dilute polymer solutions using bead-spring models: Brownian dynamics simulations and closure approximations. Thesis, Monash University, 2005.
(49) Prakash, J. R. *Macromolecules* **2001**, *34*, 3396−3411.
(50) Liu, T. W. *J. Chem. Phys.* **1989**, *90*, 5826−5842.
(51) Doyle, P. S.; Shaqfeh, E. S. G.; Gast, A. P. *J. Fluid Mech.* **1997**, *334*, 251−291.
(52) Hur, J. S.; Shaqfeh, E. S. G.; Babcock, H. P.; Smith, D. E.; Chu, S. *J. Rheol.* **2001**, *45*, 421−450.
(53) Öttinger, H. C. *Phys. Rev. A* **1989**, *40*, 2664−2671.
(54) Kumar, K. S.; Prakash, J. R. *J. Chem. Phys.* **2004**, *121*, 3886−3897.

MA702114U